


Rejuvenation of a deformed metallic glass dominated by immature shear band zones during cryogenic thermal cycling

Sailong Zhang , Jingyu Zhou , Jing Geng , Yifan Yang , Peipeng Jin , and Bo Shi *

Qinghai Provincial Key Laboratory of New Light Alloys, Qinghai Provincial Engineering Research Center of High Performance Light Metal Alloys and Forming, Qinghai University, Xining 810016, China

 (Received 8 November 2023; revised 23 February 2024; accepted 4 March 2024; published 18 March 2024)

Cryogenic thermal cycling (CTC) treatment is a promising technique to rejuvenate metallic glasses (MGs), but whose effect is usually highly dependent on the original structure. Spanning shear bands and nonspanning shear bands in deformed MGs not only have different structures, but also are situated in different strain fields, so their responses to CTC are expected to be different. In the present work, the structure, energy state, and property evolutions of the spanning and nonspanning shear bands in deformed MGs during the CTC process were investigated by experiments and molecular dynamics simulations. It was found that CTC increased the proportion of atoms with inelastic strain and induced a rejuvenation in the immature shear band zones that nevertheless led a relaxation in the mature shear band zones. This work not only deepens the understanding of the rejuvenation mechanism of deformed MGs, but also provides a unique perspective for improving their mechanical properties.

DOI: [10.1103/PhysRevB.109.104205](https://doi.org/10.1103/PhysRevB.109.104205)

I. INTRODUCTION

Metallic glasses (MGs) have excellent properties such as high strength, elasticity, and corrosion resistance [1–6]. However, their poor plasticity at room temperature has severely limited their widespread applications. The limited plasticity of MGs is primarily attributed to the shear localization behavior; namely, the plastic deformation is inhomogeneous and highly localized into shear bands (SBs). A SB consists of a core and an affected zone spanning tens to hundreds of micrometers around it [7–10]. There are significant differences of structure between SBs and the glassy matrix. For example, it was commonly believed that a SB contains a large amount of free volume compared to the glassy matrix, resulting in a soft region [11,12]. From a morphological perspective, there are generally two types of shear bands in MGs: spanning shear bands (SSBs) and nonspanning shear bands (NSBs) [13]. For a SSB, it is a well-developed and mature shear band that spans the entire MG sample. However, for a NSB, it is an undeveloped shear band that has an immature front and a relatively mature tail with a shear offset on the material surface. Then the SSB or the tail of a NSB can be regarded as a mature SB zone, but the front of a NSB can be regarded as an immature SB zone. Recently, it was found that the structure of a shear band depends on the shear strain it experiences; i.e., it becomes more disordered with the increase of shear strain [14]. Moreover, Sheng *et al.* revealed distinct differences among different segments of a shear band along its propagation direction. For example, the front and tail regions of a SB are located in different strain fields and density areas [15]. Therefore, due to different structures and surroundings, immature SB and mature SB zones may exhibit different responses to external stimuli.

Cryogenic thermal cycling (CTC) treatment is a simple, nondestructive, and promising technique for rejuvenating MGs and improving their properties [16–20]. However, there are relatively limited reports on the application of CTC to deformed MGs. Through a review of the literature, we found that CTC has diverse effects on deformed MGs. For example, our previous study revealed that CTC induced rejuvenation in a deformed MG within a certain strain range [21], while other researchers have found relaxation phenomena in cyclically thermally deformed MGs [22,23]. Obviously, there is still a lack of direct evidence to explain the underlying physical mechanisms. Recently, Das *et al.* found that the differences in the original structure can lead to completely different responses during CTC [20]. This motivates us to explore the evolutions of immature SB and mature SB zones under CTC stimulation. This will provide insights into how to achieve high rejuvenation of deformed MGs and improve their properties.

In this study, deformed MGs with different strains were subjected to CTC treatments. Both molecular dynamics (MD) simulation and experimental methods were employed to investigate the effect of CTC on deformed MGs. It was found that CTC induced relaxation in the mature SB zone while it induced rejuvenation in the immature SB zone, and finally led a transition from softening to hardening with increasing strain in deformed MGs.

II. EXPERIMENTAL METHODS

A. Materials preparation

Zr_{64.13}Cu_{15.75}Ni_{10.12}Al₁₀ (at.%) MG was chosen as the experimental alloy. The samples were prepared by arc-melting 4 N elemental constituents under a Ti-gettered argon atmosphere, followed by suction-casting into two types of Cu

*Corresponding author: boshi@qhu.edu.cn

molds with a square cross section of $2 \times 2 \text{ mm}^2$ and a diameter of 3 mm, respectively.

B. CTC process and characterization

We first performed uniaxial compressions on as-cast samples with an aspect ratio of 1:1 for different deformation amounts by using a UTM 5105 electronic universal testing machine at a strain rate of $5 \times 10^{-4} \text{ s}^{-1}$. After unloading, the deformed MGs were subjected to 20 cycles of CTC treatments [one CTC contains 1 min in room temperature (RT) environment and 1 min immersion in liquid nitrogen temperature (LN_2 , 77 K), respectively]. To characterize the structural changes of the deformed MGs with different deformation amounts before and after CTC treatments, microhardness tests were conducted using a Vickers diamond indenter with a load of 300 g and a dwell time of 15 s. The enthalpy evolution was characterized by differential scanning calorimetry (DSC, NETZSCH STA 449 F3) at a heating rate of 15 K min^{-1} . The sample was heated from RT to 713 K (the supercooled liquid region) and held for 15 min, followed by cooling to RT. The same heating program was performed again on the same sample to determine the baseline for each measurement.

C. Molecular dynamics simulations

The MD simulation of $\text{Cu}_{64}\text{Zr}_{36}$ MG model was carried out with the LAMMPS code [24]. The evolution mechanism of atoms in the SB zone during thermal cycling was investigated. As there is currently no suitable interatomic potential for $\text{Zr}_{64.13}\text{Cu}_{15.75}\text{Ni}_{10.12}\text{Al}_{10}$ MG, we have selected the $\text{Cu}_{64}\text{Zr}_{36}$ composition as a prototype in this work, owing to the availability of reliable Finnis-Sinclair type potentials [25]. The initial block containing ~ 9000 atoms was produced by quenching from the melt at a cooling rate of 0.02 K ps^{-1} . Then a rectangular sample with dimensions of $34.1 \times 5.6 \times 61.7 \text{ nm}^3$ in the x , y , and z directions, respectively, was created by replicating the initial block, resulting in a total of $\sim 7.2 \times 10^5$ atoms. To reduce the artificial boundary effect of the multiplication, the large system was further annealed at 800 K for 500 ps. To produce only two shear bands that do not affect each other as much as possible during deformation, two small notches were created in the rectangular sample to yield stress concentration on the notch and

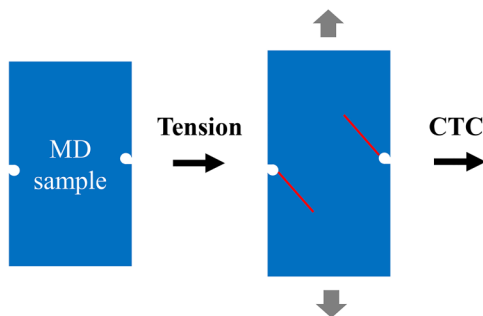


FIG. 1. Illustration of the MD simulation flow chart showing the uniaxial tension of the notched sample for different deformation amounts, followed by 5 CTCs between 100 and 400 K.

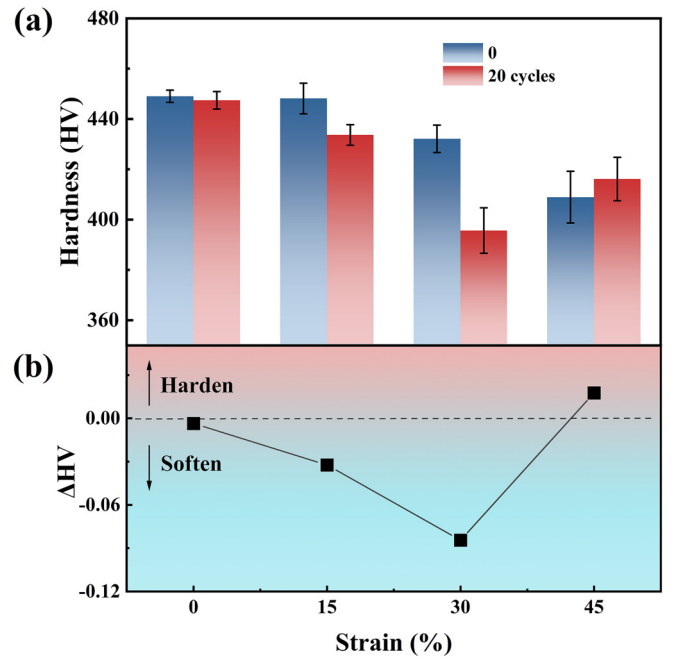


FIG. 2. (a) The microhardness values of the deformed MGs with different strains endured 0 and 20 CTC treatments (each column is the average of 20 indentations). (b) The variation of the relative hardness ΔHV with strain.

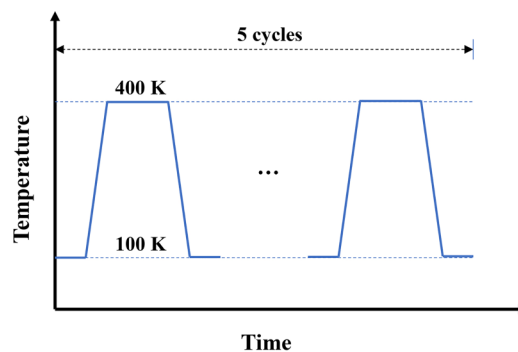
nucleate the SBs. Special notches were also designed to achieve intersected SBs.

As shown in Fig. 1, at a low temperature of 100 K, uniaxial loading with different deformation amounts was applied on the notched samples along the z direction at a constant strain rate of 10^8 s^{-1} to obtain spanning, nonspanning, and intersected SBs. Subsequently, the deformed samples underwent 5 CTCs between 100 and 400 K. The atomic shear strain, η^{Mises} [26], was calculated and visualized using OVITO software [27].

III. RESULTS AND DISCUSSION

A. Effect of CTC on the hardness of deformed MGs

Figure 2(a) displays the microhardness results of the deformed MGs with various strains treated by 0 and 20 CTCs. As indicated by the blue columns, the Vickers hardness



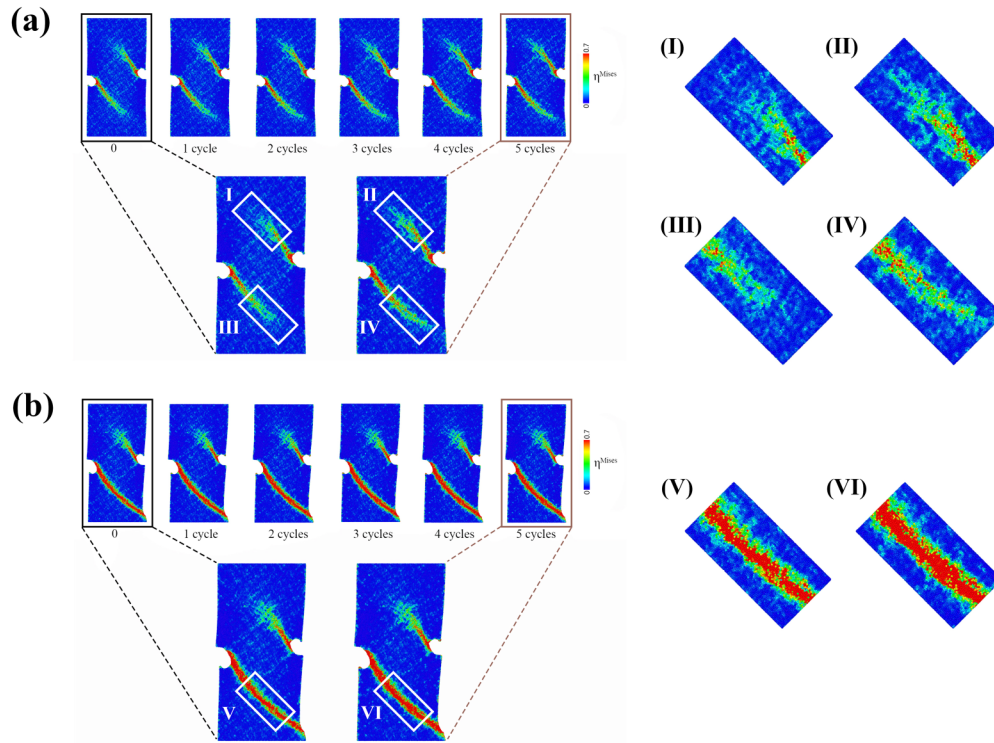


FIG. 3. Distributions of atomic shear strain η^{Mises} for MGs containing (a) two nonspanning SBs and (b) a spanning SB, which were treated with 0–5 CTCs, respectively. The regions I, III, and V marked with the boxes in the deformed MGs without CTC, and the regions II, IV, and VI marked with the boxes in the deformed MGs with 5 CTCs, are enlarged on the right side.

gradually decreases from an initial value of 449 to 409 HV as the strain increases from 0% to 45%. The decrease of hardness is mainly due to SBs produced by plastic deformation, which cause an increase in free volume content and further the softening phenomenon [11,28,29]. However, when the deformed MGs were subjected to CTC treatments, their hardness exhibited a nonmonotonic change, as shown by the red columns in Fig. 2(a). With increasing the strain from 0% to 30%, CTC treatments aggravated the softening of MGs. As can be seen, the hardness decreases from 447 to 396 HV, showing a reduction of 11.4%. Such a softening amount was significantly higher than that induced solely by SBs (a reduction of 3.8% is shown by blue columns, as the deformation increases from 0% to 30%). However, very interestingly, with the increase of the deformation amounts from 30% to 45%, the CTC-treated sample exhibited an increase in hardness from 396 to 416 HV; namely, the effect of CTC changed from softening to hardening, as shown by the red columns in Fig. 2(a). Figure 2(b) presents the relative hardness variation, ΔHV , which can be expressed as $\Delta\text{HV} = (\text{HV}_A - \text{HV}_B) / \text{HV}_B$, where HV_A and HV_B represent the hardness values after and before 20 CTC treatments, respectively. As can be seen, Fig. 2(b) provides a more intuitive demonstration for the transition of softening to hardening induced by CTC. Previous studies have suggested that CTC-induced softening in MGs is due to the presence of the differences in thermal expansion coefficients resulting from its structural heterogeneity [16,30,31]. With the temperature changing, a significant amount of internal stress is generated, which rejuvenates and softens the MGs. It should be emphasized that SBs have huge structural differences

compared to the glassy matrix [29,32–34]. Theoretically, in the deformed MGs containing SBs, more significant uncoordinated responses during CTC may lead to greater softening. However, according to our results, CTC treatments have different effects on the MGs with different deformation levels, i.e., a transition from softening to hardening with strain. Obviously, there may be a more complex physical mechanism for SB evolution during the CTC process.

B. MD simulations of CTC treatments on deformed MGs

To reveal the underlying mechanism of the transition from softening to hardening caused by CTC in MGs, we conducted MD simulations of CTC on the models with various deformation levels (Fig. 1). Firstly, we obtained two models of MGs: one model contains two NSBs [Fig. 3(a)] and the other contains a SSB [Fig. 3(b)]. Then we performed 5 cycles of CTC simulations on these two models. It has been proven that atomic shear strain η^{Mises} is a reasonable micromechanical parameter to measure the local inelastic deformation in MGs [35]. Then η^{Mises} was adopted to describe the local structure evolution at the atomic levels in the present work. Figure 3(a) represents the visualized distributions of η^{Mises} after 0–5 CTCs for the model with two NSBs. As can be seen, the local plastic zones at the front regions of these two NSBs noticeably expand along their propagation directions after CTC treatments. Clearer illustrations are also given here. For the front regions I and III marked by the boxes in Fig. 3(a) [their enlarged views are shown in (I) and (III), respectively], after 5 CTC cycles, their plastic zones exhibit significant expansion along

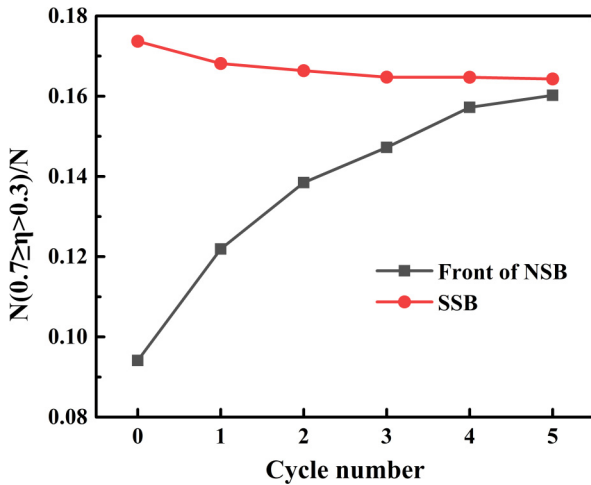


FIG. 4. The fractions of atoms with $0.7 \geq \eta^{\text{Mises}} > 0.3$ in the SSB and the front region of the NSB vary with thermal cycling.

their propagation directions, as shown in (II) and (IV), respectively. Figure 3(b) shows the evolution of η^{Mises} for the model containing a SSB (below) and a NSB (above) during CTC treatments. As can be seen, after five CTC treatments, there are almost no changes in the local plastic zone of the SSB [see (V) and (VI)]. Interestingly, for the model shown in Fig. 3(b), CTC seems to prioritize the SSB. This is very similar to the plastic deformation; for example, the reformation of a deformed MG will preferentially occur on the existing SSB due to its softer nature [13]. To summarize, our results indicate that CTC can only activate the plastic zones in the MG that solely contains NSBs. But in the MG containing the mature SSB, the plastic zones around it remain almost unchanged.

To clarify the effects of CTC on deformed MGs more essentially, the evolution of local structural damage in shear band zones during the CTC process was quantified. Previous study has shown that the atoms with $\eta^{\text{Mises}} > 0.3$ can be considered to participate in inelastic deformation, which involves shear transformation zones (STZs) [35]. However, taking into account the presence of cavities within the SBs [33], we believe that excessive atomic strain will lead to the formation of cavities when η^{Mises} exceeds a certain threshold. By employing annealing on a model containing a single mature SB, we determined that $\eta^{\text{Mises}} = 0.7$ is the upper limit for not forming cavities (for more determination details, see Note 1 in the Supplemental Material [36]). Therefore, statistical analysis on atoms with $0.7 \geq \eta^{\text{Mises}} > 0.3$ is a reasonable approach to evaluate the variations of structural damage at atomic levels. Figure 4 shows the proportion of the atoms with $0.7 \geq \eta^{\text{Mises}} > 0.3$ (for specific statistical regions, see Note 2 in the Supplemental Material [36]) as a function of thermal cycling. It can be observed that the fraction of atoms with $0.7 \geq \eta^{\text{Mises}} > 0.3$ in the front region of the NSB significantly increases with CTC number, while the change rate decreases. After the fifth cycle, the atomic fraction reaches a relatively stable value of about 0.16. Conversely, the fraction of atoms with $0.7 \geq \eta^{\text{Mises}} > 0.3$ in the mature SSB decreases with CTC number, and also tends to stabilize at the fifth cycle (the stable value is 0.164). In addition, statistical analysis on the variation of atomic proportion with CTC in different η^{Mises}

ranges was conducted (for statistical results, see Note 3 in the Supplemental Material [36]). As can be seen from Fig. S3(a) [36], CTC significantly increases the proportion of atoms with inelastic strain in the front region of NSB, i.e., increases the atomic activity. However, although a large number of atoms in the mature SSB are at high strain, their responses to CTC are relatively weak, with a slight decrease in atomic activity (Fig. S3(b) [36]). In theory, due to the differences in preparation and processing histories, the original structures of MD models and experimental MGs, as well as their responses to CTC, may not be completely identical. However, MD can indeed enlighten us to understand what possible reasons drive the changes in experimental MGs during CTC, such as the development level of shear bands.

C. Thermal analysis of deformed MGs treated with CTC

To validate the simulation results, two MG samples with a diameter of 3 mm and an aspect ratio of 1:1 were firstly compressed to a strain of 15%. Subsequently, one deformed sample served as a reference, while the other one was subjected to CTC treatments. DSC tests were carried out on the deformed MGs with and without 20 CTC treatments, to determine the structural relaxation enthalpy ΔH_{rel} . Since there are more artificial defects on the sample surface, it is often the case that SBs originate at the surface and then extend towards the interior of the MGs [37,38]. Therefore, for an appropriately deformed MG, the mature tails of SBs are mainly located near its surface, but the immature fronts of them are mainly in its interior. Then we deformed a MG sample appropriately to construct a special structure which is roughly composed of the mature SB zones mainly at the edge but the immature SB zones are mainly at the center (illustrated in the inset of Fig. 5). DSC slicing and tests were performed in the edge and center regions, respectively. As shown in Fig. 5, the ΔH_{rel} of the edge region (mainly corresponding to the mature SB zones) decreased by 32% from the original value of 6.0 to 4.1 J g⁻¹ after CTC treatment. In contrast, the center region (mainly corresponding to the immature SB zones) experienced a rejuvenation after CTC treatments, with the ΔH_{rel} increasing from the initial 6.3 to 7.6 J g⁻¹ by 21%. Therefore, it can be deduced that relaxation occurs in the mature SB zones, but rejuvenation occurs in the immature SB zones. Previous studies have demonstrated a positive correlation between ΔH_{rel} and the amount of free volume [39–41]. An increased free volume means an increase in atomic activity. Obviously, the enhancement of the proportion of high-energy atoms is the main physical process in the immature SB zones during CTC; nevertheless, the proportion of high-energy atoms decreases in the mature SB zones. Consequently, our DSC results are consistent with the MD simulation findings.

Based on a comprehensive analysis of experimental and MD simulation results, it can be concluded that CTC induces relaxation in the mature SB zones while it induces rejuvenation in the immature SB zones. Accordingly, in the stage of small strain, the plastic deformation of MGs is mainly accommodated by the formation of SBs, and the majority of them are nonspanned [13]. With the strain increasing, many of them will develop to mature spanning SBs. Because CTC leads to

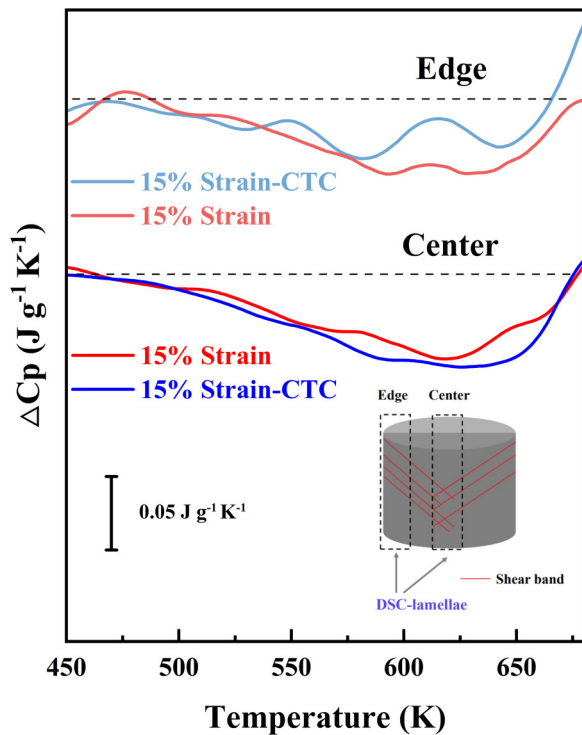


FIG. 5. DSC traces of the edge and center regions of the deformed MGs with and without CTC treatments (the inset is a schematic diagram of DSC lamellae sampling from the edge and center regions).

an increase of the atomic activity in the front of the NSBs, significant softening will occur at low strains. However, as the strain increases, CTC causes relaxation of the mature SBs, and then induces a transition from softening to hardening (as shown in Fig. 2).

Recently, Liu *et al.* revealed that the structure of a SB depends on the shear strain it experiences [14]. This implies that SSBs and the front of NSBs have different structures due to different strain levels. In addition, Das *et al.* found that CTC can homogenize the relaxation time distribution or the structural disorder, ultimately leading to a quasiequilibrium state [20]. This means that CTC will lead to rejuvenation if the original MG structure is relaxed relative to the quasiequilibrium state CTC would induce, but it will lead to relaxation if the original MG structure is more rejuvenated. Interestingly, based on the above results, our work has also confirmed this point in deformed MGs. For example, high-strain atoms in SSB are in a highly rejuvenated state, while the front of NSBs may be below the quasiequilibrium state (as shown in Fig. 4, the SSB and the front of the NSB evolve towards the same strain state from high-strain and low-strain states, respectively.). Therefore, the mature SB zones and immature SB zones exhibit two contrary behaviors, relaxation and rejuvenation, respectively.

According to our MD simulation results and previous report, the front of the NSB is embedded in and constrained by the glassy matrix, which is similar to the formation of a new phase during solid-state phase transition [42]. Moreover,

the front of the NSB has the following characteristics: along its propagation direction, the front region is extremely uneven and has significant fluctuations (shown in Fig. 3), which was also reported in previous experimental results [15,43]. It can be also found in Fig. S3(a) of the Supplemental Material [36] that the proportion of atoms in different η^{Mises} ranges varies greatly in the front of the NSB without CTC treatment. As a result, such restricted state and heterogeneous structure make the front region very sensitive to CTC treatments. Furthermore, CTC leads to larger additional atomic stresses and then greatly promoted the percentage of high-energy atoms. However, for the SSB, it has an extremely large number of high-strain atoms (Fig. 4), which possess good atomic mobility and are poised to relax under external stimuli. Therefore, in the SSB, CTC will be similar to annealing and play a relaxation role.

In addition, intersected SBs are actually important existences, which possess an original state completely different from the SSBs and NSBs mentioned above. We have found that CTC can also increase the proportion of atoms with inelastic strain and lead to a rejuvenation in the intersected zone (see Note 4 in the Supplemental Material [36]). Currently, achieving maximum rejuvenation of MGs remains a challenge. Shear bands are highly rejuvenated, but due to their low volume fraction, it is difficult for them to cause a significant rejuvenation of the whole MG sample [44]. CTC, as a popular and effective method of MG rejuvenation, has the potential to achieve a highly overall rejuvenation in a deformed MG. However, our work indicates that CTC can only rejuvenate the deformed MGs which contained more shear band fronts. Therefore, this prompts us to realize that if CTC is adopted to rejuvenate a deformed MG, the key may be to suppress the formation of mature shear bands during its deformation process.

IV. CONCLUSION

The structure, energy state, and property evolution of the immature SB and the mature SB zones in deformed MGs during CTC treatments were investigated by experiments and MD simulations. It was found that CTC increased the proportion of high-strain atoms and then induced a rejuvenation in the immature SB zones, but in the mature SB zones, CTC induced a relaxation. Within a small strain range, the remarkable softening is mainly attributed to the rejuvenation of immature SB zones induced by CTC. However, when the MG experiences a larger strain, a transition from softening to hardening induced by CTC occurs, which is mainly attributed to the relaxation of mature SB zones. These findings deepen the understanding of the rejuvenation mechanism of deformed MGs, and then provide a unique way to achieve high rejuvenation of deformed MGs.

ACKNOWLEDGMENT

This work was supported by the National Natural Science Foundation of China (Grant No. 52361026).

- [1] M. Jiang and L. Dai, Intrinsic correlation between fragility and bulk modulus in metallic glasses, *Phys. Rev. B* **76**, 054204 (2007).
- [2] D. Jang and J. R. Greer, Transition from a strong-yet-brittle to a stronger-and-ductile state by size reduction of metallic glasses, *Nat. Mater.* **9**, 215 (2010).
- [3] M. M. Trexler and N. N. Thadhani, Mechanical properties of bulk metallic glasses, *Prog. Mater. Sci.* **55**, 759 (2010).
- [4] L. Tian, Y.-Q. Cheng, Z.-W. Shan, J. Li, C.-C. Wang, X.-D. Han, J. Sun, and E. Ma, Approaching the ideal elastic limit of metallic glasses, *Nat. Commun.* **3**, 609 (2012).
- [5] W. H. Wang, The elastic properties, elastic models and elastic perspectives of metallic glasses, *Prog. Mater. Sci.* **57**, 487 (2012).
- [6] M. Telford, The case for bulk metallic glass, *Mater. Today* **7**, 36 (2004).
- [7] R. Maaß, Beyond serrated flow in bulk metallic glasses: What comes next? *Metall. Mater. Trans. A* **51**, 5597 (2020).
- [8] F. A. Davani, S. Hilke, H. Rösner, D. Geissler, A. Gebert, and G. Wilde, On the shear-affected zone of shear bands in bulk metallic glasses, *J. Alloys Compd.* **837**, 155494 (2020).
- [9] L. Q. Shen, P. Luo, Y. C. Hu, H. Y. Bai, Y. H. Sun, B. A. Sun, Y. H. Liu, and W. H. Wang, Shear-band affected zone revealed by magnetic domains in a ferromagnetic metallic glass, *Nat. Commun.* **9**, 4414 (2018).
- [10] R. Maaß, P. Birckigt, C. Borchers, K. Samwer, and C. A. Volkert, Long range stress fields and cavitation along a shear band in a metallic glass: The local origin of fracture, *Acta Mater.* **98**, 94 (2015).
- [11] J. Pan, Q. Chen, L. Liu, and Y. Li, Softening and dilatation in a single shear band, *Acta Mater.* **59**, 5146 (2011).
- [12] J. Bokeloh, S. V. Divinski, G. Reglitz, and G. Wilde, Tracer measurements of atomic diffusion inside shear bands of a bulk metallic glass, *Phys. Rev. Lett.* **107**, 235503 (2011).
- [13] R. T. Qu, Z. Q. Liu, G. Wang, and Z. F. Zhang, Progressive shear band propagation in metallic glasses under compression, *Acta Mater.* **91**, 19 (2015).
- [14] C. Liu, Y. Ikeda, and R. Maaß, Strain-dependent shear-band structure in a Zr-based bulk metallic glass, *Scr. Mater.* **190**, 75 (2021).
- [15] H. Sheng, D. Şopu, S. Fellner, J. Eckert, and C. Gammer, Mapping shear bands in metallic glasses: From atomic structure to bulk dynamics, *Phys. Rev. Lett.* **128**, 245501 (2022).
- [16] S. V. Ketov, Y. H. Sun, S. Nachum, Z. Lu, A. Checchi, A. R. Beraldin, H. Y. Bai, W. H. Wang, D. V. Louzguine-Luzgin, M. A. Carpenter *et al.*, Rejuvenation of metallic glasses by non-affine thermal strain, *Nature (London)* **524**, 200 (2015).
- [17] W. Guo, J. Saida, M. Zhao, S. Lü, and S. Wu, Unconspicuous rejuvenation of a Pd-based metallic glass upon deep cryogenic cycling treatment, *Mater. Sci. Eng. A* **759**, 59 (2019).
- [18] Z. Long, P. Tao, L. Kong, G. Wang, S. Huang, S. Wen, H. He, Z. Huang, X. Zhu, X. Xu *et al.*, Effect of cryogenic thermal cycling on the microstructure and mechanical properties of Zr-based bulk metallic glasses, *Mater. Sci. Eng. A* **863**, 144513 (2023).
- [19] Z. Wang, P. Huang, X. Fan, and F. Wang, Heterogeneity dependent cryogenic thermal cycling behavior of metallic glasses: A potential energy landscape perspective, *Intermetallics* **159**, 107935 (2023).
- [20] A. Das, E. M. Dufresne, and R. Maaß, Structural dynamics and rejuvenation during cryogenic cycling in a Zr-based metallic glass, *Acta Mater.* **196**, 723 (2020).
- [21] S. Zhang, J. Zhou, J. Wang, B. Shi, and P. Jin, Significant rejuvenation of a deformed metallic glass contributed by shear band affected zones during cryogenic cycling, *Mater. Lett.* **326**, 132988 (2022).
- [22] A. Hassanpour, M. Vaidya, S. V. Divinski, and G. Wilde, Impact of cryogenic cycling on tracer diffusion in plastically deformed Pd₄₀Ni₄₀P₂₀ bulk metallic glass, *Acta Mater.* **209**, 116785 (2021).
- [23] B. S. Li, S. Xie, and J. J. Kruzic, Toughness enhancement and heterogeneous softening of a cryogenically cycled Zr–Cu–Ni–Al–Nb bulk metallic glass, *Acta Mater.* **176**, 278 (2019).
- [24] S. Plimpton, Fast parallel algorithms for short-range molecular dynamics, *J. Comput. Phys.* **117**, 1 (1995).
- [25] M. I. Mendeleev, D. J. Sordelet, and M. J. Kramer, Using atomistic computer simulations to analyze x-ray diffraction data from metallic glasses, *J. Appl. Phys.* **102**, 043501 (2007).
- [26] F. Shimizu, S. Ogata, and J. Li, Theory of shear banding in metallic glasses and molecular dynamics calculations, *Mater. Trans.* **48**, 2923 (2007).
- [27] A. Stukowski, Visualization and analysis of atomistic simulation data with OVITO—the Open Visualization Tool, *Modell. Simul. Mater. Sci. Eng.* **18**, 015012 (2010).
- [28] H. Bei, S. Xie, and E. P. George, Softening caused by profuse shear banding in a bulk metallic glass, *Phys. Rev. Lett.* **96**, 105503 (2006).
- [29] R. Maaß, K. Samwer, W. Arnold, and C. A. Volkert, A single shear band in a metallic glass: Local core and wide soft zone, *Appl. Phys. Lett.* **105**, 171902 (2014).
- [30] B. Shang, W. Wang, A. L. Greer, and P. Guan, Atomistic modelling of thermal-cycling rejuvenation in metallic glasses, *Acta Mater.* **213**, 116952 (2021).
- [31] S. Di, Q. Wang, J. Zhou, Y. Shen, J. Li, M. Zhu, K. Yin, Q. Zeng, L. Sun, and B. Shen, Enhancement of plasticity for FeCoBSiNb bulk metallic glass with superhigh strength through cryogenic thermal cycling, *Scr. Mater.* **187**, 13 (2020).
- [32] A. L. Greer, Y. Q. Cheng, and E. Ma, Shear bands in metallic glasses, *Mater. Sci. Eng., R* **74**, 71 (2013).
- [33] C. Liu, V. Roddatis, P. Kenesei, and R. Maaß, Shear-band thickness and shear-band cavities in a Zr-based metallic glass, *Acta Mater.* **140**, 206 (2017).
- [34] V. Schmidt, H. Rösner, M. Peterlechner, G. Wilde, and P. M. Voyles, Quantitative measurement of density in a shear band of metallic glass monitored along its propagation direction, *Phys. Rev. Lett.* **115**, 035501 (2015).
- [35] D. Şopu, M. Stoica, and J. Eckert, Deformation behavior of metallic glass composites reinforced with shape memory nanowires studied via molecular dynamics simulations, *Appl. Phys. Lett.* **106**, 211902 (2015).
- [36] See Supplemental Material at <http://link.aps.org/supplemental/10.1103/PhysRevB.109.104205> for local structural damage determination in MD simulations, selection of statistical region for η^{Mises} , statistics on the variation of atomic proportion in different η^{Mises} ranges, and changes of η^{Mises} before and after CTC in intersected shear bands model.
- [37] B. Yang, M. L. Morrison, P. K. Liaw, R. A. Buchanan, G. Wang, C. T. Liu, and M. Denda, Dynamic evolution of nanoscale shear

- bands in a bulk-metallic glass, *Appl. Phys. Lett.* **86**, 141904 (2005).
- [38] S. X. Song, X. L. Wang, and T. G. Nieh, Capturing shear band propagation in a Zr-based metallic glass using a high-speed camera, *Scr. Mater.* **62**, 847 (2010).
- [39] J. Pan, Y. X. Wang, Q. Guo, D. Zhang, A. L. Greer, and Y. Li, Extreme rejuvenation and softening in a bulk metallic glass, *Nat. Commun.* **9**, 560 (2018).
- [40] W. Guo, R. Yamada, and J. Saida, Rejuvenation and plasticization of metallic glass by deep cryogenic cycling treatment, *Intermetallics* **93**, 141 (2018).
- [41] W. Song, X. Meng, Y. Wu, D. Cao, H. Wang, X. Liu, X. Wang, and Z. Lu, Improving plasticity of the $Zr_{46}Cu_{46}Al_8$ bulk metallic glass via thermal rejuvenation, *Sci. Bull.* **63**, 840 (2018).
- [42] Z. Liu, R. Li, G. Wang, S. Wu, X. Lu, and T. Zhang, Quasi phase transition model of shear bands in metallic glasses, *Acta Mater.* **59**, 7416 (2011).
- [43] L.-Q. Shen, J.-H. Yu, X.-C. Tang, B.-A. Sun, Y.-H. Liu, H.-Y. Bai, and W.-H. Wang, Observation of cavitation governing fracture in glasses, *Sci. Adv.* **7**, 14 (2021).
- [44] Y. Sun, A. Concustell, and A. L. Greer, Thermomechanical processing of metallic glasses: Extending the range of the glassy state, *Nat. Rev. Mater.* **1**, 16039 (2016).